

## Phase Locking between Two All-Optical Quantum Memories

Fumiya Okamoto,<sup>1</sup> Mamoru Endo<sup>1,\*</sup>, Mikiyoshi Matsuyama,<sup>1</sup> Yuya Ishizuka,<sup>1</sup> Yang Liu,<sup>2</sup>Rei Sakakibara,<sup>1</sup> Yosuke Hashimoto,<sup>1</sup> Jun-ichi Yoshikawa,<sup>1,†</sup> Peter van Loock,<sup>3</sup> and Akira Furusawa<sup>1,‡</sup><sup>1</sup>Department of Applied Physics, School of Engineering, The University of Tokyo, 7-3-1 Hongo, Bunkyo-ku, Tokyo 113-8656, Japan<sup>2</sup>State Key Laboratory of Quantum Optics and Quantum Optics Devices, Collaborative Innovation Center of Extreme Optics, Institute of Opto-Electronics, Shanxi University, Taiyuan 030006, China<sup>3</sup>Institute of Physics, Johannes Gutenberg-Universität Mainz, Staudingerweg 7, 55099 Mainz, Germany

(Received 16 September 2020; accepted 2 December 2020; published 31 December 2020)

Optical approaches to quantum computation require the creation of multimode photonic quantum states in a controlled fashion. Here we experimentally demonstrate phase locking of two all-optical quantum memories, based on a concatenated cavity system with phase reference beams, for the time-controlled release of two-mode entangled single-photon states. The release time for each mode can be independently determined. The generated states are characterized by two-mode optical homodyne tomography. Entanglement and nonclassicality are preserved for release-time differences up to 400 ns, confirmed by logarithmic negativities and Wigner-function negativities, respectively.

DOI: 10.1103/PhysRevLett.125.260508

Optical quantum information processing based on continuous variables, where quantum information is encoded in traveling electromagnetic field modes, is one of the most promising approaches to efficient, practical quantum computation [1]. In particular, the generation of scalable continuous-variable cluster states (CVCSs)—highly entangled multimode Gaussian states—was demonstrated recently in a time-domain multiplexing scheme [2–5]. Moreover, an experiment was recently reported in which 100 Gaussian gate operations were executed via such a temporal resource state at a high clock rate [6]. The remaining challenge toward universal fault-tolerant quantum computation including quantum error correction is to incorporate non-Gaussian states into the time-multiplexed CVCS. A promising implementation for fault-tolerant universal quantum computation has been proposed [7], where non-Gaussian quantum states, such as cubic-phase states [8] and Gottesman-Kitaev-Preskill states [9], are injected into the time-multiplexed CVCS. However, the bottleneck here is that currently such non-Gaussian states can be only probabilistically generated in a heralding fashion. As a possible remedy, optical quantum-state sources with phase-locked quantum memories can be employed to temporarily store and eventually release the optical wave packets (WPs) at appropriate times ( $t_1, t_2, \dots$ ), as illustrated in Fig. 1.

Although storage of a single-photon state, which is one of the fundamental nonclassical states of light, has already been demonstrated in various ways [10–13] and some of these schemes can be exploited as an on-demand quantum-state resource [12,13], the state verification is typically done by coincidence measurements in these experiments. Only in recent years, nonclassical optical states were kept

in a quantum memory to an extent that allowed one to preserve the negative values of the states' Wigner functions [14–17]. Here the negativity of the Wigner function determined by homodyne tomography indicates strong nonclassicality, which, however, is easily degraded by loss or phase fluctuations. Most notably, a novel all-optical concatenated cavity system (CCS) composed of a memory and a shutter cavity may serve as an elementary tool, especially for CVCS-based universal quantum computation, because of the system's low-loss configuration for various wavelength regimes. A single CCS was shown to store a nonclassical single-photon state, preserving its Wigner-function negativity [16]. Subsequently, two CCSs were utilized in order to synchronize the release

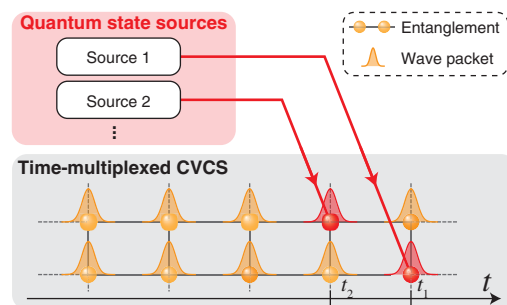


FIG. 1. Possible concept for fault-tolerant universal quantum computation based on a time-multiplexed CVCS as proposed in Ref. [7], where the WPs of Gaussian states are entangled with each other. In this figure, the lines between WPs denote entanglement links. WPs of quantum states of light, which are generated by phase-locked nonclassical, non-Gaussian state sources, are injected into the CVCS in a controlled fashion at certain times  $t = t_1, t_2, \dots$

of two single photons and to create an entangled Hong-Ou-Mandel state verified by full homodyne tomography [18]. More recently, the CCS was extended to store and release a non-Gaussian, phase-sensitive, single-mode superposition state by introducing phase probe beams into the CCS [17]. The ultimate next step toward applications such as CVCS quantum computing is now to synchronize multiple phase-sensitive memories by introducing a phase-locking mechanism between them and to release the stored WPs independently in a time-controlled fashion.

Here, we demonstrate phase locking between two timing controllable phase-sensitive memories. This enables us to release, in a controlled fashion, single-photon two-mode entangled states created inside the memories by a heralding mechanism. More specifically, we create quasi-on-demand optical quantum states such as  $\alpha|0\rangle_1|1\rangle_2 + \beta e^{i\theta}|1\rangle_1|0\rangle_2$ , where  $\alpha, \beta, \theta \in \mathbb{R}$ ,  $|n\rangle$  represents an  $n$ -photon state (here  $n = 0, 1$ ), and the subscripts 1 and 2 denote mode numbers. The system can tailor the parameters ( $\alpha, \beta, \theta$ ), in principle, arbitrarily and it can independently control the release times ( $t_1, t_2$ ) for the two optical modes. Here in the main text, we focus on the simplest symmetric  $\theta = 0$  case,  $(\alpha, \beta, \theta) = (1/\sqrt{2}, 1/\sqrt{2}, 0)$ , for which we confirmed that the two modes maintain their quantum coherence and nonclassicality during storage times of up to 400 ns. Some additional experimental results with a different choice of parameters for the released two-mode quantum states such as  $(1/\sqrt{3}, \sqrt{2}/3, \pi)$ ,  $(1/\sqrt{2}, 1/\sqrt{2}, \pi)$ , and  $(1/\sqrt{2}, 1/\sqrt{2}, 5\pi/6)$ , including different emission timings, are presented in the Supplemental Material [19]. The phase-controlled synchronization among multimode quantum systems as demonstrated here can be directly utilized for fault-tolerant large-scale quantum computation with CVCSs as proposed in Ref. [7]. In our experiment, the two-mode states have fixed photon number one, similar to a one-photon two-mode qubit state (so-called dual-rail qubit). In other words, our experiment can be probably considered the first all-optical demonstration for a quasi-on-demand generation of an arbitrary dual-rail qubit. Note that similar demonstrations were made before based on solid-state and atom quantum memories [22,23]. However, we stress that this particular manifestation of our Letter highlights only a narrow aspect of our system, which can be more generally applied to higher photon and mode numbers as required in CVCS quantum computation. As for higher photon numbers, it is already theoretically known that we can directly generate arbitrary two-mode states with a fixed photon number,  $\sum_{n=0}^N c_{n,N-n}|n\rangle_1|N-n\rangle_2$ , where  $c_{k,l} \in \mathbb{C}$  [24]. This corresponds to encoding a single spin of arbitrary size into two optical field modes [25]. The resulting larger Hilbert spaces may then also contain bosonic error correction codes, for example,  $\alpha(|4\rangle_1|0\rangle_2 + |0\rangle_1|4\rangle_2)/\sqrt{2} + \beta|2\rangle_1|2\rangle_2$  adapted for protection against photon loss [26]. By adding more photons or modes, NOON states for quantum-enhanced metrology [27,28] or gain for quantum

error correction [29] may be producible in a controlled way. To our knowledge, this is the first demonstration of phase-locking multimode optical quantum systems with time-controlled memories, verified by two-mode optical homodyne tomography.

Let us explain how to generate the two-mode quantum states  $\alpha|0\rangle_1|1\rangle_2 + \beta e^{i\theta}|1\rangle_1|0\rangle_2$  by means of two nondegenerate optical parametric oscillators (NOPOs), linear optics, and single-photon detection. The (unnormalized) initial four-mode state  $|\psi_{\text{initial}}\rangle$  generated from the two NOPOs can be written as

$$|\psi_{\text{initial}}\rangle = \sum_{n_1=0}^{\infty} q_1^{n_1} |n_1\rangle_{s_1} |n_1\rangle_{i_1} \otimes \sum_{n_2=0}^{\infty} q_2^{n_2} |n_2\rangle_{s_2} |n_2\rangle_{i_2}, \quad (1)$$

where  $s, i$  represent ‘‘signal’’ and ‘‘idler’’ modes, and  $q_{1,2}$  include the pump amplitudes for the NOPOs. The idler modes from the two NOPOs are combined at a beam splitter. When a single photon is detected at one of the outputs of the BS, the signal fields are projected onto a two-mode entangled state  $|\psi\rangle$ ,

$$\begin{aligned} & {}_{i_1}\langle 0|_{i_2}\langle 1|\hat{U}_{i_1,i_2}(t_{\text{BS}}, r_{\text{BS}})|\psi_{\text{initial}}\rangle \\ &= t_{\text{BS}}q_2|0\rangle_{s_1}|1\rangle_{s_2} + r_{\text{BS}}q_1|1\rangle_{s_1}|0\rangle_{s_2} \\ &\propto \alpha|0\rangle_{s_1}|1\rangle_{s_2} + \beta e^{i\theta}|1\rangle_{s_1}|0\rangle_{s_2} = |\psi\rangle, \end{aligned} \quad (2)$$

where  $\hat{U}_{i_1,i_2}(t_{\text{BS}}, r_{\text{BS}})$  is a BS operator acting on modes  $i_1$  and  $i_2$ . The parameters  $t_{\text{BS}}, r_{\text{BS}} \in \mathbb{C}$  are transmission and reflection coefficients of the BS, respectively, satisfying  $|t_{\text{BS}}|^2 + |r_{\text{BS}}|^2 = 1$ . Finally, the parameters  $(\alpha, \beta, \theta)$  in Eq. (2) are determined by  $t_{\text{BS}}, r_{\text{BS}}$ , and  $q_{1,2}$ . Note that the state projection via single-photon detection at one output port of the BS is expressed by  ${}_{i_1}\langle 0|_{i_2}\langle 1|\hat{U}_{i_1,i_2}(t_{\text{BS}}, r_{\text{BS}})$  under a weak-pumping condition ( $|q_{1,2}| \ll 1$ ), while the detector employed in the experiment was an avalanche photodiode (APD). This method can be extended to the generation of two-mode states with higher photon numbers [24]. Note that, in the following, we omit the subscripts for simplicity.

Figure 2 shows how to combine the above heralding method with the CCSs and how to control the release times of the two-mode-state WPs. Nondegenerate parametric down-conversion occurs inside each memory cavity (memory 1, 2). The shutters in the CCSs are concatenated shutter cavities (SCs) transmitting either the signal or the idler for suitably tuned resonance frequencies. At the beginning, the SCs are only open for the idlers, thus the signals are stored in each memory [Fig. 2(a)]. The emitted idlers are combined at the BS with phase  $\theta$ . When an idler photon is detected, the resulting state  $|\psi\rangle$  emerges in the memory cavities [Fig. 2(b)]. Each shutter is opened after appropriate waiting times ( $t_1, t_2$ ) by shifting each SC’s resonance frequency correspondingly; then the signal WPs are released independently [Fig. 2(c)]. Because the two

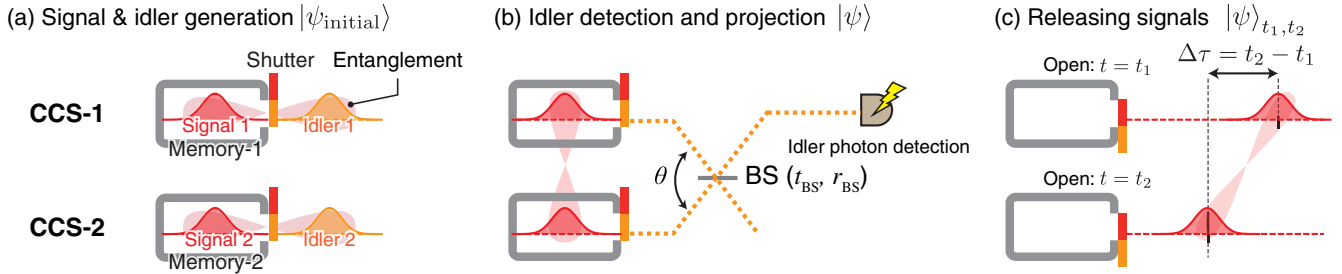


FIG. 2. Conceptual diagram of release timing control by two quantum memories. (a) Generation of entanglement between signal (red) and idler (orange) modes in each memory cavity [Eq. (1)]. Only the idler modes are released. (b) Idler detection and projection [Eq. (2)]. Arbitrary entangled states can be generated by tuning the beam splitting ratio  $(t_{\text{BS}}, r_{\text{BS}})$  and the phase between two phase references from each memory  $(\theta)$ . (c) Quasi-on-demand release of the entangled state by opening the shutters for the signal modes independently  $(t_1, t_2)$ .

memories are phase locked via the idler probe beams, the output two-mode state can keep its phase relation, although the releases of the two WPs will typically happen at different times.

The experimental apparatus is illustrated in Fig. 3 and further details can be found in the Supplemental Material [19]. We select the signal and the idler fields to be separated in frequency by the free spectral range (FSR) of the memory cavities, which corresponds to 214 MHz (or 0.5-pm wavelength difference). In order to separate the signal and the idler fields, which are collinearly emitted from the same output coupler of each SC, frequency separating cavities are employed. Then, the idler modes are combined at a BS for setting the superposition parameters  $(\alpha, \beta, \theta)$ . The average power in each probe beam is approximately 2 mW. One of the BS output fields is guided toward an APD through cascaded filtering cavities to

eliminate unwanted light. The probe beams for the idler and the signal are injected into the memory cavities, while the optical frequency of the idler probe is up-shifted with the corresponding acousto-optic frequency shifter (AOFS-2) by 214 MHz, which corresponds to the FSR of the memory cavity. To probe the phase of the signal and the idler fields in the CCSs, the phase relation among the pump, signal probe, and idler probe beams are locked via phase-sensitive parametric amplification. These probe beams are used for phase locking the idler beams at the BS and for the signal-homodyne measurements. The probe beams are essential for the phase-sensitive memories, but they should be absent during storage and release of the signal quantum states, because strong probe beams would disturb the heralding and homodyne signals. Optical switches based on acousto-optic modulators (AOS 1, 2) with periods of 200  $\mu\text{s}$  are used as a beam chopper. More

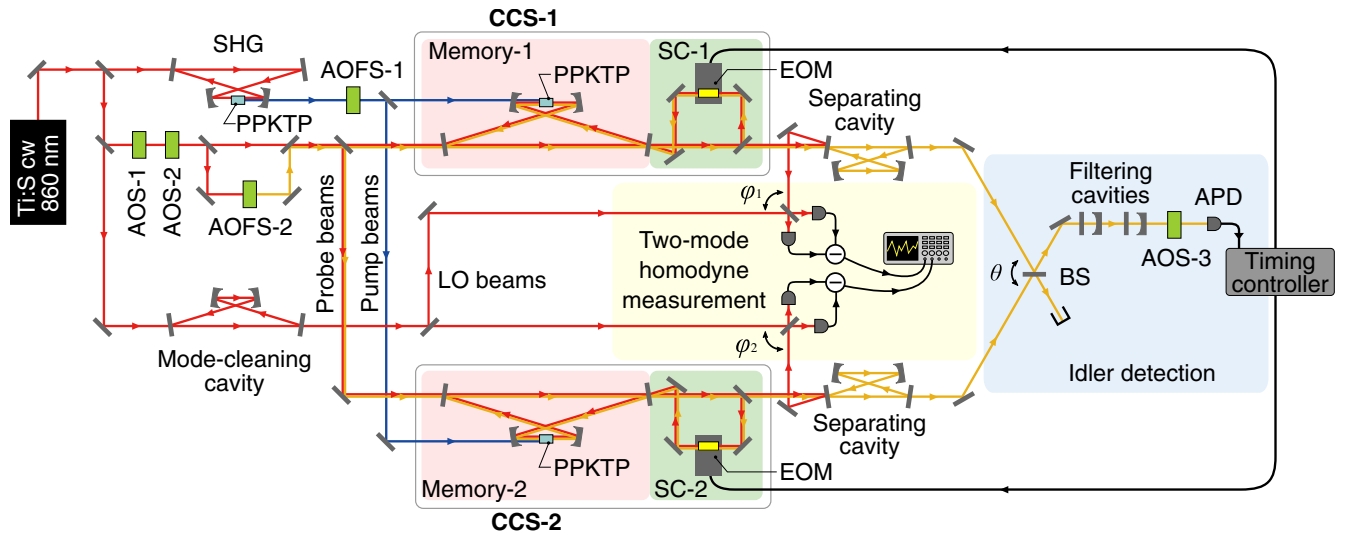


FIG. 3. Experimental apparatus. The light source is a 860 nm continuous-wave (cw) Ti:Sapphire laser. Red and orange lines stand for the signal and idler beams, respectively. Blue lines represent the pump beams. Black lines stand for electric signals. Memory, memory cavity based on NOPO with a cavity length of 1.4m; SC, shutter cavity with a length of 0.7m; SHG, second harmonic generation to generate the pump beams (430 nm); PPKTP, periodically poled  $\text{KTiOPO}_4$  crystal (type-0); AOFSs, acousto-optic frequency shifters; AOSs, acousto-optic switches; BS, beam splitter for setting superposition parameters  $(\alpha, \beta)$ .

details on the measurement sequence can be found in [19]. As long as the probe beams are on, the system locks the cavities and the phase relations. Storage and release of the quantum states as well as homodyne measurements are done when the probe beams are off.

In the main text, we refer to a BS with a reflectivity of 50% and a phase  $\theta = 0$ . In the Supplemental Material [19], we show results with other BSs and we lock to various phases corresponding to different two-mode quantum states. In order for each memory's counts to be the same, the pump powers into the memory cavities are suitably adjusted (approximately 2 mW each). The average heralding rate of each CCS was set to 200 counts per second (cps) and the residual count rate by stray light is at a 10 cps level. After receiving the heralding signal and predetermined waiting times ( $t_1, t_2$ ), a timing controller based on a field-programmable gate array sends trigger signals to open the SCs. Each shutter is opened by applying a high voltage (900 V) to an electro-optic modulator (EOM), which corresponds to a resonance frequency shift of 214 MHz. The opening duration of each shutter is set to be 500 ns, which is sufficiently longer than the WP size. The released signal fields are measured by two optical homodyne detectors. Note that the resonance frequency of the memory cavities is detuned (300 kHz) from the frequency of the local oscillator (LO) beams to suppress the occurrence of unwanted photons stored by the memory, which is caused by the scattering of the strong LO beams. This detuning leads to a rotation of the released quantum states for  $t_1 \neq t_2$  [19].

We performed balanced optical homodyne measurements for the signal fields around the heralding signals

at various LOs' phases  $\varphi_1, \varphi_2$ , where 3000 pairs of waveforms for each of 49 homodyne bases ( $\varphi_1, \varphi_2$ ) were acquired by an oscilloscope. The LOs' phases were stabilized via the heterodyne beat notes between the signal probe and the LO beams.

In a preliminary experiment, the envelopes of the signal WPs for the single-photon states were determined by homodyne measurements [16,20,21]. The envelopes of the released WP amplitudes for different emission times are shown in Fig. 4(a). The emission times are correctly shifted and the shape of the envelopes is independent of the storage times. The idler-photon detection event corresponds to 0 ns [Fig. 2(b)]. The occurring gap of about 40 ns between  $t = 0$  and the rising edges of the envelopes when  $t_1 = t_2 = 0$  is due to a latency of the electronics. Any nonzero positive values before the photon emissions correspond to leakage of the memories, but the contribution of this leakage can be ignored [16].

As a final result, we stored and released two-mode entangled states to infer their density matrices. The density matrices for the WPs in Fig. 4(a) are shown in Fig. 4(b). The off-diagonal terms  $|0, 1\rangle\langle 1, 0|$  and  $|1, 0\rangle\langle 0, 1|$  indicate the presence of entanglement. The diagonal and the off-diagonal terms decrease at the same rate. This means that the system preserves the phase information even though small intracavity losses degrade the quantum states during their storage. Figures 4(a) and 4(b) give evidence that the CCSs are indeed sufficiently phase locked and that the memories release entangled states in the various target WPs preserving their phase relations. The storage times are 1.42  $\mu\text{s}$  (CCS 1) and 1.29  $\mu\text{s}$  (CCS 2). The logarithmic negativities  $E(\hat{\rho}_{AB}) = \log_2 \|\hat{\rho}_{AB}^{TB}\|$  are calculated and

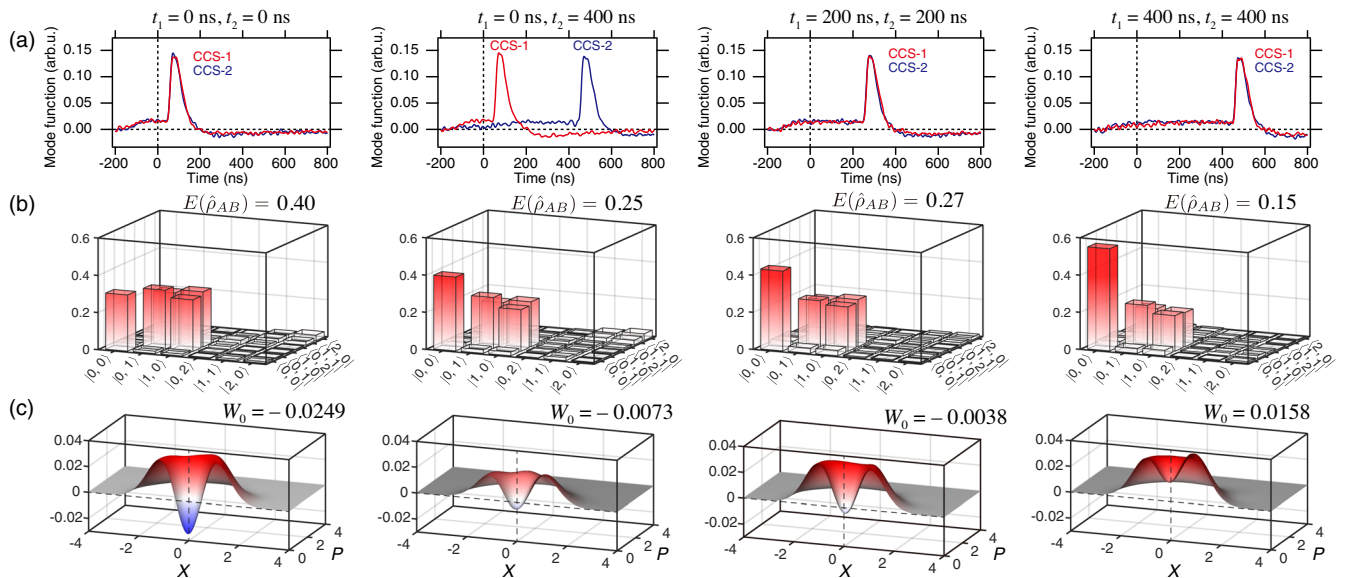


FIG. 4. Experimental results. (a) Experimentally determined envelopes of the released WP amplitudes from CCS-1 (red traces) and CCS-2 (blue traces). The idler-photon detection event corresponds to 0 ns. (b) Absolute values of density matrix elements with experimentally determined logarithmic negativities. (c) Calculated cross sections of the Wigner function  $W(X, P, X, P)$  with the values at the origin. The emission times ( $t_1, t_2$ ) are (0, 0), (0, 400), (200, 200), and (400, 400) ns from the left to the right columns.

presented in Fig. 4(b) to confirm the entanglement [30–32], where  $\|\cdot\|$  and  $\cdot^{T_B}$  represent the trace norm and partial transpose, respectively. Here, the calculation of the logarithmic negativity is done in the renormalized subspace spanned by  $\{|0,0\rangle, |0,1\rangle, |1,0\rangle, |1,1\rangle\}$  [19]. A nonzero value of the logarithmic negativity indicates that the state is entangled, which is still observable in our experiment even when  $t_1 = t_2 = 400$  ns. Two-mode Wigner functions  $W(x_1, p_1, x_2, p_2)$  are calculated from the density matrices to confirm that our system is able to preserve strong nonclassicality. The cross sections  $W(X, P, X, P)$  and the values at the phase-space origin ( $W_0$ ) are shown in Fig. 4(c). The negative values around the origin indicate that our CCSs can store and release fragile, nonclassical states for emission times (0,0),(0,400),(200,200) ns. Even though the negativities of the Wigner function can be easily degraded, our system successfully preserves them. The standard deviations of the phase fluctuation range from  $25^\circ$  to  $30^\circ$ , which are estimated from the reconstructed density matrices. Such a relatively large fluctuation can also be caused by the pump power fluctuation or the phase noise of the laser and not only by the phase locking. The above values are considered as upper limits of the actual phase fluctuations. A detailed discussion on this aspect can be found in [19].

In conclusion, we experimentally demonstrated the coherent synchronization and hence the quasi-on-demand release of two-mode quantum states of light by means of two time-controlled, all-optical, phase-locked memories. For practical quantum computation as proposed in Ref. [7], the storage time must be longer than the inverse of the generation rate. In this case, this means the required storage time is on the order of milliseconds, which is a factor of 1000 longer than the value realized in our experiment. However, multiple CCSs can be synchronized and multiplexed based on our proposed method to mitigate this condition. Also, improving the rate by modifying the CCS as well as employing photon-number resolving detectors under a strong pump condition are possible remedies. Via full control over the phase relation of the two memories, the release times of the signal modes can be independently adjusted to keep the entanglement and the nonclassicality of the optical quantum states. We experimentally prepared a representative set of single-photon dual-rail qubit states quasi-on-demand. Our scheme is also directly applicable to the controlled creation of optical states with more modes and more photons including logical qubits of bosonic quantum error correction codes with a fixed photon number sufficiently exceeding 1. Since the exploitation of optical quantum states with nonzero photon-number variance depends, in particular, on the reliable manipulation of their relative phases, our scheme also provides a fundamental solution for this broader class of applications. Therefore, ultimately, it is applicable to optical measurement-based, fault-tolerant universal quantum information processing.

This work was partly supported by JSPS KAKENHI (Grants No. 18H01149 and No. 18H05207), CREST (Grant No. JPMJCR15N5) of JST, UTokyo Foundation, and donations from Nichia Corporation of Japan. F. O. and Y. H. acknowledge support from Advanced Leading Graduate Course for Photon Science (ALPS). M. M. acknowledges support from Forefront Physics and Mathematics Program to Drive Transformation (FoPM). P. v. L. acknowledges QLinkX (BMBF, Germany) and ShoQC (Quantero, EU/BMBF).

\*endo@ap.t.u-tokyo.ac.jp

†yoshikawa@ap.t.u-tokyo.ac.jp

‡akiraf@ap.t.u-tokyo.ac.jp

- [1] S. Lloyd and S. L. Braunstein, *Phys. Rev. Lett.* **82**, 1784 (1999).
- [2] S. Yokoyama, R. Ukai, S. C. Armstrong, C. Sornphiphatpong, T. Kaji, S. Suzuki, J. Yoshikawa, H. Yonezawa, N. C. Menicucci, and A. Furusawa, *Nat. Photonics* **7**, 982 (2013).
- [3] J. Yoshikawa, S. Yokoyama, T. Kaji, C. Sornphiphatpong, Y. Shiozawa, K. Makino, and A. Furusawa, *APL Photonics* **1**, 060801 (2016).
- [4] W. Asavanant, Y. Shiozawa, S. Yokoyama, B. Charoensombutamon, H. Emura, R. N. Alexander, S. Takeda, J. Yoshikawa, N. C. Menicucci, H. Yonezawa, and A. Furusawa, *Science* **366**, 373 (2019).
- [5] M. V. Larsen, X. Guo, C. R. Breum, J. S. Neergaard-Nielsen, and U. L. Andersen, *Science* **366**, 369 (2019).
- [6] W. Asavanant, B. Charoensombutamon, S. Yokoyama, T. Ebihara, T. Nakamura, R. N. Alexander, M. Endo, J. Yoshikawa, N. C. Menicucci, H. Yonezawa, and A. Furusawa, *arXiv:2006.11537*.
- [7] R. N. Alexander, S. Yokoyama, A. Furusawa, and N. C. Menicucci, *Phys. Rev. A* **97**, 032302 (2018).
- [8] K. Miyata, H. Ogawa, P. Marek, R. Filip, H. Yonezawa, J. I. Yoshikawa, and A. Furusawa, *Phys. Rev. A* **93**, 022301 (2016).
- [9] D. Gottesman, A. Kitaev, and J. Preskill, *Phys. Rev. A* **64**, 012310 (2001).
- [10] A. I. Lvovsky, B. C. Sanders, and W. Tittel, *Nat. Photonics* **3**, 706 (2009).
- [11] C. Clausen, I. Usmani, F. Bussi eres, N. Sangouard, M. Afzelius, H. de Riedmatten, and N. Gisin, *Nature (London)* **469**, 508 (2011).
- [12] T. Zhong, J. M. Kindem, J. G. Bartholomew, J. Rochman, I. Craiciu, E. Miyazono, M. Bettinelli, E. Cavalli, V. Verma, S. W. Nam, F. Marsili, M. D. Shaw, A. D. Beyer, and A. Faraon, *Science* **357**, 1392 (2017).
- [13] A. Seri, A. Lenhard, D. Riel ander, M. G undogan, P. M. Ledingham, M. Mazzer, and H. de Riedmatten, *Phys. Rev. X* **7**, 021028 (2017).
- [14] E. Bimbard, R. Boddada, N. Vitrant, A. Grankin, V. Parigi, J. Stanojevic, A. Ourjoumtsev, and P. Grangier, *Phys. Rev. Lett.* **112**, 033601 (2014).
- [15] M. Bouillard, G. Boucher, J. F. Ortas, B. Pointard, and R. Tualle-Brouri, *Phys. Rev. Lett.* **122**, 210501 (2019).

- [16] J. Yoshikawa, K. Makino, S. Kurata, P. van Loock, and A. Furusawa, *Phys. Rev. X* **3**, 041028 (2013).
- [17] Y. Hashimoto, T. Toyama, J. Yoshikawa, K. Makino, F. Okamoto, R. Sakakibara, S. Takeda, P. van Loock, and A. Furusawa, *Phys. Rev. Lett.* **123**, 113603 (2019).
- [18] K. Makino, Y. Hashimoto, J. Yoshikawa, H. Ohdan, T. Toyama, P. van Loock, and A. Furusawa, *Sci. Adv.* **2**, e1501772 (2016).
- [19] See Supplemental Material at <http://link.aps.org/supplemental/10.1103/PhysRevLett.125.260508> for the methods, preliminary experiment, experimental results with various parameters, and precise calculations for the losses, which includes Refs. [16–18,20,21].
- [20] A. MacRae, T. Brannan, R. Achal, and A. I. Lvovsky, *Phys. Rev. Lett.* **109**, 033601 (2012).
- [21] O. Morin, C. Fabre, and J. Laurat, *Phys. Rev. Lett.* **111**, 213602 (2013).
- [22] I. Usmani, C. Clausen, F. Bussi eres, N. Sangouard, M. Afzelius, and N. Gisin, *Nat. Photonics* **6**, 234 (2012).
- [23] N. Kalb, A. Reiserer, S. Ritter, and G. Rempe, *Phys. Rev. Lett.* **114**, 220501 (2015).
- [24] J. Yoshikawa, M. Bergmann, P. van Loock, M. Fuwa, M. Okada, K. Takase, T. Toyama, K. Makino, S. Takeda, and A. Furusawa, *Phys. Rev. A* **97**, 053814 (2018).
- [25] J. Schwinger, *On Angular Momentum*, Tech. Rep. (Nuclear Development Associates, Inc., Oak Ridge, TN, 1952).
- [26] I. L. Chuang, D. W. Leung, and Y. Yamamoto, *Phys. Rev. A* **56**, 1114 (1997).
- [27] X. M. Jin, C. Z. Peng, Y. Deng, M. Barbieri, J. Nunn, and I. A. Walmsley, *Sci. Rep.* **3**, 1779 (2013).
- [28] M. M uller, H. Vural, C. Schneider, A. Rastelli, O. G. Schmidt, S. H ofling, and P. Michler, *Phys. Rev. Lett.* **118**, 257402 (2017).
- [29] M. Bergmann and P. van Loock, *Phys. Rev. A* **94**, 012311 (2016).
- [30] M. B. Plenio, *Phys. Rev. Lett.* **95**, 090503 (2005).
- [31] G. Vidal and R. F. Werner, *Phys. Rev. A* **65**, 032314 (2002).
- [32] J. Eisert, Ph. D. thesis, University of Potsdam, Germany, 2001.